*Korean J. Chem. Eng.*, 36(6), 869-879 (2019)
DOI: 10.1007/s11814-019-0283-1

pISSN: 0256-1115
eISSN: 1975-7220

# Simultaneous adsorption of $Cd^{2+}$ and methylene blue from aqueous solution using xanthate-modified baker's yeast

**Mingyao Song*, Zhengyang Duan***, Ronggao Qin**,†, Xiaojun Xu*, Shuli Liu*, Shumin Song*, Mengjiao Zhang*, Yue Li*, and Jiemei Shi***

*Faculty of Environmental Science and Engineering, Kunming University of Science and Technology, Kunming 650500, P. R. China
**Faculty of Land Resource Engineering of Kunming University of Science and Technology, Kunming 650500, P. R. China
***Faculty of Geography and Tourism Management, Chuxiong Normal University, Chuxiong 675000, P. R. China
(*Received 15 October 2018 • accepted 27 April 2019*)

**Abstract**−Xanthate-modified baker's yeast (XMBY) was successfully synthesized by grafting xanthate groups onto the surface of baker's yeast and was used for the simultaneous adsorption of cadmium ($Cd^{2+}$) and methylene blue (MB) from aqueous solution. Scanning electron microscopy-energy dispersive spectroscopy (SEM-EDS) and Fourier transform infrared spectroscopy (FTIR) were used to characterize the synthesized adsorbent. The results indicated that the sulfur groups were successfully introduced onto the surface of the baker's yeast and participated in the adsorption processes. The kinetic and isotherm data showed good correlations with the pseudo-second-order model and the Langmuir model, respectively. The equilibrium time and the maximum values obtained from the two models were 40 min, 239.8 mg/g for $Cd^{2+}$ and 300 min, 64.45 mg/g for MB, respectively. The thermodynamic analysis ($\Delta G<0$, $\Delta H>0$, $\Delta S>0$) demonstrated that the adsorption processes of $Cd^{2+}$ and MB onto the XMBY were endothermic and spontaneous. In the binary-component solution ($Cd^{2+}$ and MB), the adsorption capacity for MB was almost unaffected by the presence of $Cd^{2+}$ and interestingly, the adsorption capacity for $Cd^{2+}$ increased in the presence of MB. Overall, these results indicated that XMBY could be a promising adsorbent for the treatment of wastewater containing both $Cd^{2+}$ and MB.

Keywords: Baker's Yeast, Adsorption, Cadmium, Methylene Blue, Wastewater

## INTRODUCTION

Heavy metals and dyes are two hazardous pollutants that usually coexist in the effluents of many industries [1]. For example, the wastewater of dye manufacturing, textile, as well as pulp and paper industries contains both types of contaminants. Dyes are used as a coloring agent to colorize products, and heavy metals are used as a mordant in the dyeing process [2,3]. Due to their toxicity, perdurability, carcinogenicity and mutagenicity, the water quality has deteriorated significantly in recent years [4,5]. Cadmium, as an indispensable element, is commonly used in the manufacture of nickel-cadmium batteries; however, in effluents, it pollutes the environment and negatively affects human health. Many diseases are related to cadmium exposure, such as toxic pulmonary edema, liver damage and skeletal deformities [5]. Meanwhile, cadmium has similar properties as other heavy metals, i.e., stability, degradation resistance and simple bio-magnification through the food chain. With the rapid development of various chemical industries, cadmium pollution is increasing. Methylene blue (MB) is a type of cationic dye that is widely used in printing, paper-making and the textile industries. However, when MB is present in the water environment, it will limit the light penetration into the water layer, thus affecting the dissolved oxygen concentration in the water and the photosynthesis conditions of aquatic organisms; eventually, aquatic ecosystems become polluted [5,6]. To prevent further deterioration of the environment, it is imperative to deal with the pollution caused by $Cd^{2+}$ and MB. Hence, the objective of this study was to find an effective and energy-saving method to simultaneously remove $Cd^{2+}$ and MB.

Many studies have been published on the removal of heavy metals or dyes in a single-component system, but very few studies focused on the simultaneous removal of both dyes and heavy metals in binary-component or multi-component systems [4,18,29,33]. However, as has been pointed out, heavy metals and dyes often coexist in a variety of wastewaters. Due to significant differences in the physical and chemical properties of both pollutants, the treatment of complex wastewaters becomes more difficult and challenging. Therefore, the simultaneous removal of heavy metals and organic dyes from wastewater with an economical, simple and efficient method has become an important research topic in the field of wastewater treatment. Various treatment techniques for the removal of heavy metals and dyes have been reported in recent years, such as chemical precipitation, membrane separation, ion exchange, and adsorption [1,2,7-11]. Among these, adsorption has been considered as a suitable method to deal with environmental pollution due to its high efficiency, low cost and simplicity of operation [12]. Numerous researchers used adsorption to remove heavy metals and dyes, e.g., Zhao et al. conducted experiments to study the adsorp-

†To whom correspondence should be addressed.
E-mail: rgqinkmust@sina.com

tion mechanism of EDTA-cross-linked β-cyclodextrin to adsorb $Cu^{2+}$, $Cd^{2+}$, Safranin O, crystal violet, and MB [3]. Liu et al. used agro-processing waste oil-tea shell for the adsorption of $Cu^{2+}$, $Pb^{2+}$ and $Cd^{2+}$ from water and studied the adsorption property of the material in a solution containing MB dye and metal ions [14]. Zhu et al. investigated functionalized polyacrylamide by xanthate for $Cr^{6+}$ removal [15]. Li et al. fabricated a novel magnetic peach gum bead (MPGB) biosorbent for adsorbing cationic MB dye [20]. Song et al. synthesized an efficient peach gum polysaccharide-based amine-rich gel (ARG) adsorbent for the removal of anionic dye (methyl orange and amaranth) from water [21]. Mohammad et al. studied the adsorption of $Cd^{2+}$, $Cu^{2+}$, and MB by using date pits as a solid adsorbent [16]. The obtained results showed that the adsorption technique had an effect on the removal of dyes and heavy metals.

The adsorbents used during the adsorption process are diverse. Different substrates can be modified using different modification means, and the modified materials will have diverse separation effects on the target pollutants. Baker's yeast has always been used as a biological fermentation agent and loosening agent for the production of bread. Large quantities of negatively charged organic functional groups, such as hydroxyl, amino and phosphoryl are present in the cell wall of baker's yeast, which contains amylase, protein, lipid, chitin and other compounds. Hence, yeast biomass has generally some attraction with cations in the solution in a certain pH range. Due to its many excellent properties, such as a particle diameter larger than common biosorbents, an internal component security, easy to combine with metal ions and low cost [17-19], baker's yeast has been widely investigated in wastewater treatment. However, due to its small amount of functional groups on the surface and poor mechanical properties, the adsorption performance is low; therefore, many researchers modified baker's yeast to achieve better adsorption capability of contaminants in wastewater. For example, Xia et al. used $MnO_2$ functional baker's yeast to adsorb $Cd^{2+}$ [19] and Xu et al. investigated the removal of $Ca^{2+}$, $Cd^{2+}$, and $Pb^{2+}$ using magnetic $Fe_3O_4$ baker's yeast [32]. Modified baker's yeast has high removal efficiency for pollutants.

In this study, a biosorbent based on baker's yeast was synthesized. The resulting xanthate-modified baker's yeast (XMBY) was then used to adsorb $Cd^{2+}$ and MB in a single-component solution or binary-component solution. To understand the adsorption behavior and intrinsic mechanism, Fourier transform infrared spectroscopy (FTIR), scanning electron microscopy (SEM), energy dispersive spectroscopy (EDS), X-ray diffraction (XRD), and Zeta potential measurements were conducted. The effects of the pH and adsorbent dosage were investigated. The pseudo-first-order model, the pseudo-second-order model, the Langmuir model and the Freundlich model were utilized to fit the kinetic and isotherm data, respectively. The thermodynamics were also evaluated to explore the effect of temperature on the overall adsorption process. Finally, a mechanism for the simultaneous removal of heavy metals and dyes by the XMBY is proposed.

## EXPERIMENTAL SECTION

### 1. Materials and Reagents

The baker's yeast used in the experiments was purchased from Angle Yeast Co., Ltd. (Hubei, China). The $Cd(NO_3)_2{\cdot}4H_2O$ and MB powders were used as sources for the metal and dye ions; NaOH and $CS_2$ were also utilized in the modification process. These four reagents and other chemicals were of analytical grade and were purchased from Sinopharm Chemical Reagent Co., Ltd. (Shanghai, China). Ultrapure water was used for all experiments and 0.1 mol/L $HNO_3$ and 0.1 mol/L NaOH were used to adjust the range of pH.

### 2. Modification of Baker's Yeast

The xanthate-modification process was conducted according to the method described by Bediako et al. [22], and the modification conditions were optimized via the response surface method. Considering that $CS_2$ has a low boiling point (46.5 °C) and high volatility, the reaction process was divided into two stages. During the first stage, $CS_2$ reacted with NaOH to form an ionized water-soluble substance with high reactivity (HO·CS·SNa), which reacted with the baker's yeast easily in the second stage. NaOH (7.58 g) and 100 ml of ultrapure water were mixed in a 250 ml conical flask to obtain a 7.58% NaOH solution; then, 3.78 ml $CS_2$ was dropwise added to the 7.58% NaOH solution and the mixture was stirred for 20 min at 30 °C in a temperature-controlled shaker at a speed of 120 rpm. Subsequently, 2 g dried baker's yeast was added to the conical flask. The conical flask with the aforementioned materials was stirred for

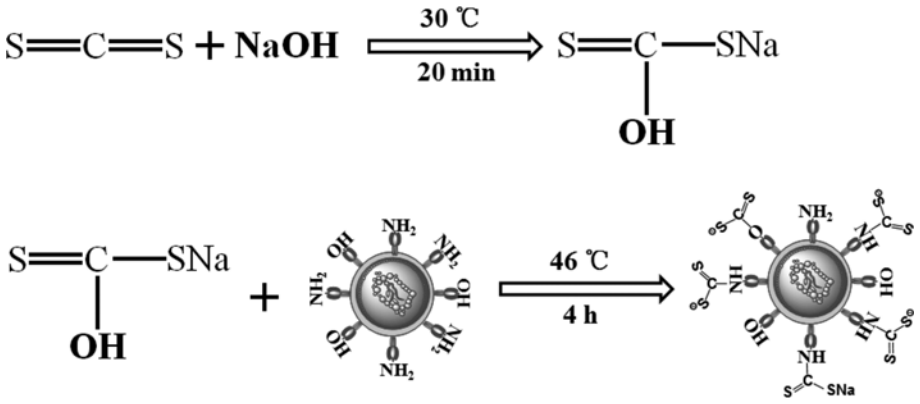


**Fig. 1. The synthetic diagram of XMBY.**

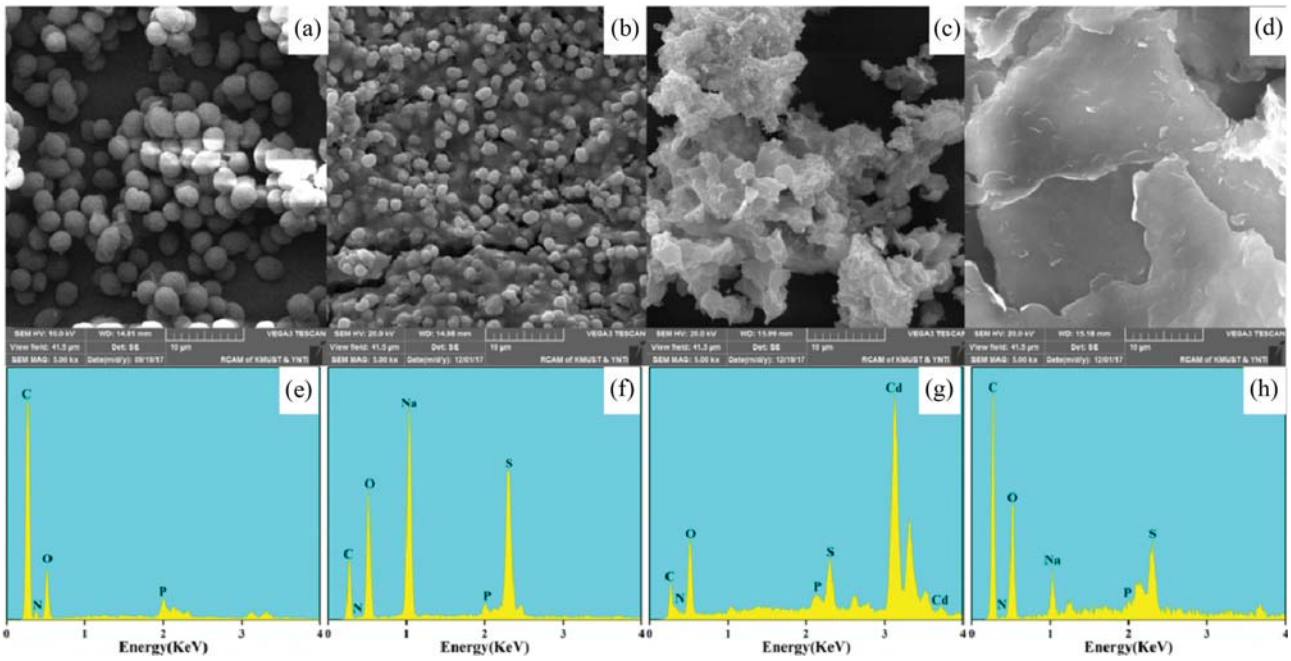


**Fig. 2. SEM images and EDS spectra of baker's yeast ((a) and (e)), XMBY ((b) and (f)), XMBY-$Cd^{2+}$ ((c) and (g)), XMBY-MB ((d) and (h)).**

4 h at 46 °C in the shaker at the same speed of 120 rpm. After stirring, the conical flask was taken out and the light orange solution was poured into a 500 ml beaker. The precipitation was washed with distilled water and ethanol until the pH was about 7. The product was freeze-dried for 48 h at −40 °C and the final XMBY was obtained for the batch experiments. The synthetic diagram is presented in Fig. 1.

### 3. Batch Adsorption Experiments

Stock solutions of 1,000 mg/L $Cd^{2+}$ and 1,000 mg/L MB were prepared by dissolving specific amounts of $Cd(NO_3)_2{\cdot}4H_2O$ or MB powders in ultrapure water, respectively. Batch adsorption studies were conducted in 250 ml conical flasks and shaken on an intelligent temperature-controlled shaker. 100 ml of $Cd^{2+}$ solution at concentrations of 5-150 mg/L and 100 ml of MB solution at concentrations of 5-100 mg/L were stirred at 120 rpm in the shaker with appropriate amounts of XMBY for 40 min and 300 min, respectively. The pH ranges of the adsorption of $Cd^{2+}$ and MB were adjusted to 3-8 and 3-10, respectively. Adsorption kinetics were conducted at $Cd^{2+}$ concentrations of 25 to 150 mg/L and MB concentrations of 10 to 100 mg/L at a temperature of 25 °C and the designated pH, respectively. Adsorption isotherms were conducted at temperatures ranging from 25 °C to 35 °C at different initial concentrations. The binary-component batch experiments were conducted under appropriate conditions with initial concentrations of 10, 25, 50, and 100 mg/L for the $Cd^{2+}$ solutions and 5, 10, 25 and 50 mg/L for the MB solutions, respectively.

All tests were conducted in triplicate and average values are presented. In all experiments, the concentrations of $Cd^{2+}$ and MB were measured via atomic absorption spectrophotometer and ultraviolet (UV)-spectrophotometer. The adsorption capacities and removal efficiencies of the adsorbent were calculated according to the following two equations:

$$q_e = \frac{(C_0 - C_e)}{M} V \tag{1}$$

$$\text{Removal}(\%) = \frac{(C_0 - C_e)}{C_0} \times 100\% \tag{2}$$

where $C_0$ (mg/L) and $C_e$ (mg/L) are the concentrations of the adsorbates in the initial and adsorption equilibrium, respectively; M (g) is the amount of adsorbent and V (L) is the volume of the adsorbed solution.

## RESULTS AND DISCUSSION

### 1. Characterization

1-1. SEM and EDS

The SEM and EDS images of the baker's yeast, XMBY, XMBY-$Cd^{2+}$, and XMBY-MB samples are shown in Fig. 2. Fig. 2(a) shows the baker's yeast cells, most of which are oval whereas some of them are round. The diameter of the particles is about 3-5 μm. After the synthetic process (Fig. 2(b)), a large number of baker's yeast granules aggregate to form a flat and compact matrix, and the morphology and distribution of the baker's yeast can still be seen on the substrate. Furthermore, most of the surface of the XMBY is exposed outside; this provides more active binding sites for $Cd^{2+}$ and MB and thus enhances the adsorption performance. Fig. 2(c) and Fig. 2(d) display the SEM images of the final products of $Cd^{2+}$ and MB adsorbed by the XMBY, respectively. After adsorbing $Cd^{2+}$, the originally flat XMBY becomes irregular and dispersed and many apertures appear on the surface; however, the granular structure of the baker's yeast can still be noticed. The XMBY-MB sample appears lamellar with a transparent structure and is very different from the XMBY-$Cd^{2+}$ sample, thus demonstrating that not only surface adsorption occurs in the adsorption process of $Cd^{2+}$ and MB onto the

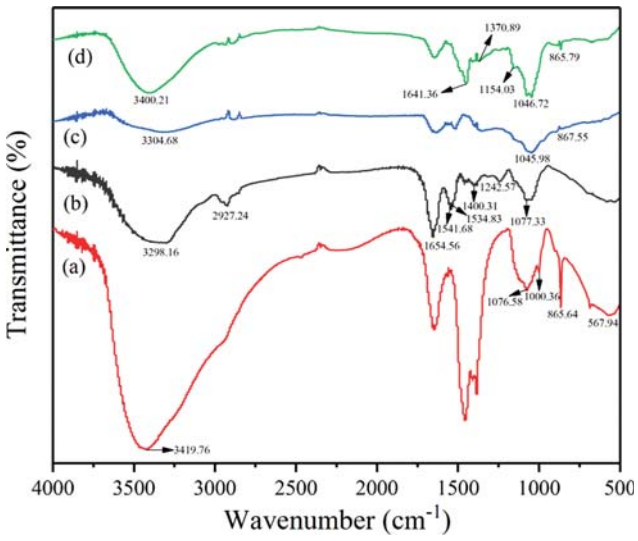


**Fig. 3. FTIR spectra of XMBY (a), baker's yeast (b), XMBY-$Cd^{2+}$ (c), XMBY-MB (d).**

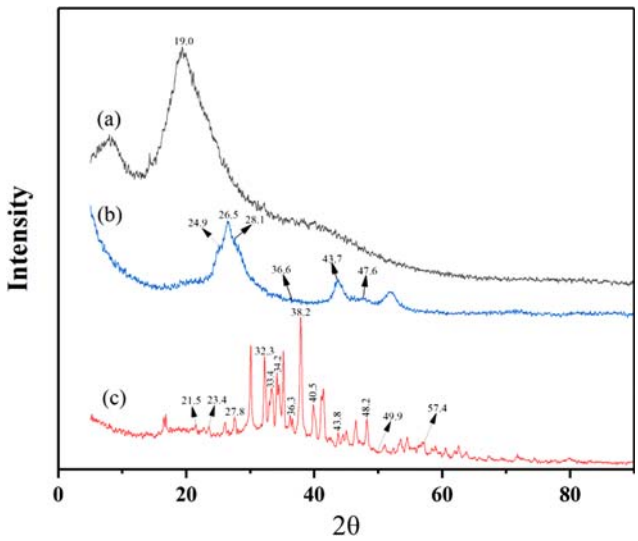


**Fig. 4. XRD patterns of baker's yeast (a), XMBY-$Cd^{2+}$ (b) and XMBY (c).**

XMBY. The EDS images further explain the aforementioned synthesis and adsorption processes. Sulfur and sodium are observed in Fig. 2(f), indicating that the sulfur groups were already introduced to the surface of the baker's yeast. The peak of cadmium in the XMBY-$Cd^{2+}$ samples only (Fig. 2(g)) shows that some complexes of XMBY with $Cd^{2+}$ emerged after adsorption; moreover, the peak of sodium disappeared, which shows some ion-exchange reactions have occurred in the adsorption process of $Cd^{2+}$ by XMBY.

1-2. FTIR

The FTIR spectra of the baker's yeast, XMBY, XMBY-$Cd^{2+}$, and XMBY-MB are shown in Fig. 3. The broad band ranging from 3,245 to 3,440 $cm^{-1}$ is caused by the overlapping -OH/$NH_2$ stretching vibration. Some distinct peaks are visible in the FTIR spectra of the baker's yeast (Fig. 3(b)). The peak at 2,927.24 $cm^{-1}$ shows the C-H stretching vibration; the peaks at 1,654.56 and 1,400.31 $cm^{-1}$ are attributed to the asymmetric and symmetric stretching vibration of C=O in the ionic carboxylic groups [11,22]; the peaks at 1,541.68 and 1,534.83 $cm^{-1}$ are due to the stretching vibration of the -$NH_2$ groups; the peaks at 1,242.57 and 1,077.33 $cm^{-1}$ correspond to the C-N stretching vibration and C-O stretching vibration [11,13,16,22], respectively. After the synthesis (Fig. 3(a)), the peak of the -OH/$NH_2$ stretching vibration shifts from 3,298.16 $cm^{-1}$ in the baker's yeast to 3,419.76 $cm^{-1}$ in the XMBY, which indicates that the -OH/$NH_2$ groups have combined with $CS_2$. New peaks at 1,076.58, 1,000.36, and 865.64/567.94 $cm^{-1}$ are observed and correspond to $\gamma_{S\text{-}C\text{-}S}$, $\gamma_{C=S}$, and $\gamma_{C\text{-}S}$, respectively [11,22]. This indicates that the sulfur groups were successfully loaded onto the surface of the baker's yeast. Several changes are noticeable in the spectra of XMBY-$Cd^{2+}$ and XMBY-MB (Fig. 3(c), 3(d)). The peaks of -OH/$NH_2$ shift to 3,304.68 and 3,400.21 $cm^{-1}$, the peaks of S-C-S shift to 1,045.95 and 1,046.72 $cm^{-1}$, and the peaks of C-S shift to 867.55 and 865.79 $cm^{-1}$, demonstrating that sulfur groups, hydroxyl groups, and amino groups are involved in the adsorption of $Cd^{2+}$ and MB onto the XMBY. In addition, the peak at 1,154.03 $cm^{-1}$ is attributed to C-N, the peak at 1,370.89 $cm^{-1}$ is due to the aromatic ring vibration, which is sensitive to the interaction with the azo bond, and the peak at 1,641.36 $cm^{-1}$ is the C=N [32]. The C-N stretching vibration and C=N are both contained in the structure of MB, which further illustrates that MB has successfully been adsorbed onto the surface of the XMBY.

1-3. XRD

The XRD patterns of the baker's yeast, XMBY, XMBY-$Cd^{2+}$, and XMBY-MB at $2\theta$ are shown in Fig. 4. The baker's yeast has a distinct diffraction peak at $2\theta$=19.0° and a similar phenomenon was also reported by Xia et al. [19]. After synthesis, obvious changes can be noticed in the XRD pattern of the XMBY; many abrupt peaks appear mainly in the range of $2\theta$=20-50°, which indicates that the yeast cells became amorphous [22]. Moreover, most peaks are coincident with $Na_2CO_3$·!$H_2O$ (21.5, 32.2, 33.4, 34.2, 36.3, 38.2, 43.8, 48.2°; JCPDF#08-0448) and $CS_2$ bonds (23.4, 27.8, 40.5, 49.9, 57.4°; JCPDF#76-0064), indicating that the XMBY is a well-crystallized material and that sulfur groups exist on the XMBY. After $Cd^{2+}$ sorption, changes can be seen in Fig. 4(b). Three intense peaks are clearly visible (26.5, 43.7, and 51.9°), indicating that some crystallization properties reappeared and the crystalline $Cd^{2+}$ ions easily penetrate the amorphous parts of the XMBY and are subsequently adsorbed [22]. Thus, in the spectrum of the XMBY-$Cd^{2+}$, peaks relating to the CdS bonds (24.9, 26.5, 28.1, 36.6, 43.7, and 47.6°; JCPDF#41-1049) emerged, demonstrating that the $Cd^{2+}$ ions have attached to specific binding sites of the XMBY. All the above-mentioned data originate from the diffraction file library and the Joint Committee on Powder Diffraction Standards (JCPDS) database [22].

**2. Batch Experiments**

2-1. Effect of pH

As has been repeatedly reported, a key factor, and perhaps the most important parameter that has been investigated for adsorbing contaminants, is the pH of the solution (adsorbate). Therefore, a series of equilibrium experiments were conducted to study the effect of the pH on the adsorption of $Cd^{2+}$ and MB onto XMBY for a wide range of pH values from 3 to 8 for $Cd^{2+}$ and 3 to 10 for MB.

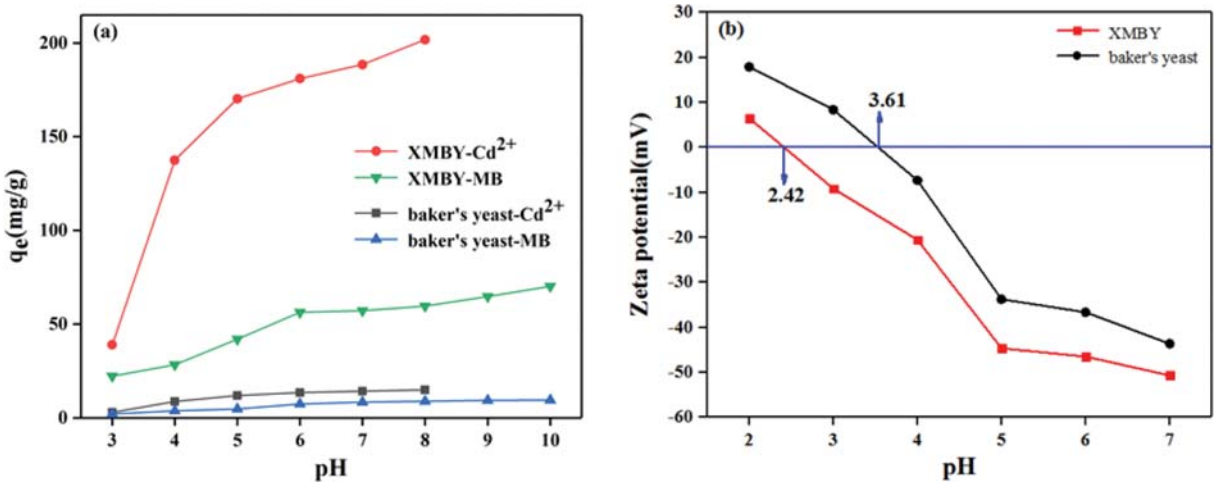


**Fig. 5. Effect of pH on the adsorption of $Cd^{2+}$ and MB onto the baker's yeast and the XMBY (a) and on the Zeta potential of the baker's yeast and the XMBY (b) (reaction conditions: $Cd^{2+}$ and MB concentrations of 50 mg/L with XMBY dosage of 0.2 g/L at 25 °C, pH 3-8 for $Cd^{2+}$ and 3-10 for MB, contact time are 40 min for $Cd^{2+}$ and 300 min for MB).**

The results are shown in Fig. 5(a). The adsorption capacities of the baker's yeast for $Cd^{2+}$ and MB increased with increasing pH from 3 to 15 mg/g and from 2.13 to 9.5 mg/g, respectively. However, the adsorption capacities of the XMBY increased significantly from 39 to 201.75 mg/g for $Cd^{2+}$ and from 22.25 to 70.25 mg/g for MB. These results indicate that the XMBY exhibits better adsorption performance for adsorbing $Cd^{2+}$ and MB than the baker's yeast.

The lower adsorption capacities at a lower pH are due to the higher positive charge density of the surface sites, which enhance the electrostatic repulsion between the positive charge of the adsorbent surface and the cation contaminants. Further evidence explains this phenomenon. It is well known that the xanthate group is unstable in a strongly acidic solution and easily dissociates from the surface of the modified baker's yeast. Otherwise, an overabundance of $H^+$ exists at low pH, which protonates the amino groups on the surface of the XMBY [23,34]. Furthermore, as a type of cationic dye, MB generates cationic pigments ($MB^+$) in an aqueous solution, thereby inhibiting the adsorption of MB in low pH solutions [24].

$$R\text{-}NH_2 + H^+ \leftrightarrow R\text{-}NH_3^+ \text{ (amino protonation)}$$

With increasing pH, an increasing number of hydroxyl groups facilitate the deprotonation of the amino groups, which is beneficial for the adsorption caused by the electrostatic attraction between both oppositely charged ions [6,25].

$$R\text{-}NH_2 + OH^- \leftrightarrow R\text{-}NH^- + H_2O \text{ (amino deprotonation)}$$
$$R\text{-}NH^- + MB^+ \leftrightarrow R\text{-}NH\text{-}MB \text{ (ionic pair formation)}$$

The zeta potential values of the baker's yeast and the XMBY are shown in Fig. 5(b). With increasing pH, the zeta potential values of the baker's yeast and the XMBY decreased due to the de-protonation effect. The point of zero charge ($pH_{pzc}$) of the XMBY was lower than that of the baker's yeast (2.42 for XMBY and 3.61 for baker's yeast), indicating that the xanthate treatment introduced the negatively charged functional groups (sulfur groups) on the surface of baker's yeast. Moreover, the repeated vacuum freeze-drying treatment of the yeast cells resulted in the destruction of the outer layer of the yeast cell walls; the negatively charged intracellular functional groups (i.e., phosphoryl group) also became more exposed. A greater number of negatively charged functional groups likely caused an increase in the electrostatic attraction between the XMBY and $Cd^{2+}$, MB. In the pH range of 3-7, the absolute values of the zeta potential of the XMBY were larger than those of the baker's yeast, which indicates that the electrostatic adsorption capacities of the cationic $Cd^{2+}$ and MB were higher for the XMBY than for baker's yeast in this pH range.

When $pH<pH_{pzc}$, the surface of the XMBY was charged positively and the abundant $H^+$ competed for adsorption sites with $Cd^{2+}$ and MB on the surface of the adsorbent; thus, the adsorption capacity was lower. In contrast, when $pH>pH_{pzc}$, the adsorption capacity was higher. This may be due to the deprotonation effect, which led to the negatively charged surface of the XMBY and enhanced the electrostatic attraction between $Cd^{2+}$ or MB and the XMBY.

With a further increase in the pH, the adsorption capacities reached the maximum values of 201.75 mg/g for $Cd^{2+}$ and 70.25 mg/g for MB at pH values of 8 and 10, respectively. However, in a previous study on $Cd^{2+}$ speciation, a diagram indicated that at pH> 8.0, the main form of $Cd^{2+}$ was $Cd(OH)_2$ [5]. Therefore, considering the suitable pH condition for the subsequent mixing experiments, a pH value of 7 was chosen for adsorbing $Cd^{2+}$ and MB.

2-2. Effect of Adsorbent Dosage

The results of the adsorbent dosage tests are shown in Fig. 6. The overall data show two major trends. When the added adsorbent dosage ranged from 0.05 to 0.2 g/L, the removal efficiency increased from 6.9% to 76% for $Cd^{2+}$ and from 3.95% to 22.5% for MB, respectively. At this stage, the increasing adsorbent dosage provides sufficient surface area and available binding sites for $Cd^{2+}$ and MB to form chelation and electrostatic attraction with the XMBY. When the adsorbent dosage was continuously increased from 0.2 to 1 g/L, the removal efficiency increased slowly from 76% to 85.7% for $Cd^{2+}$ and from 22.5% to 30.54% for MB, respectively.

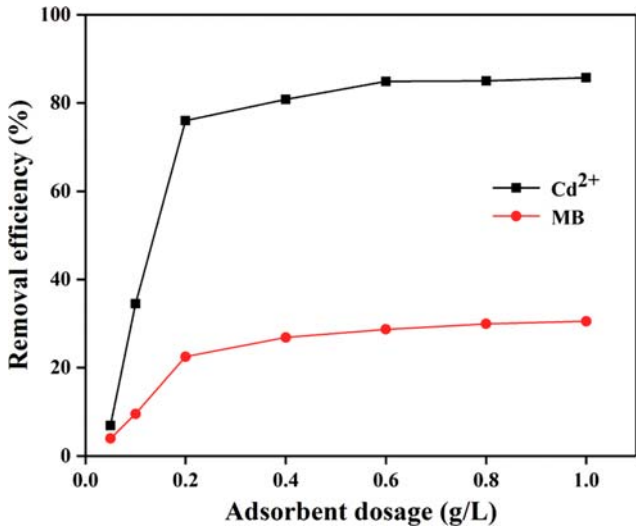


**Fig. 6. Effect of XMBY dosage on $Cd^{2+}$ and MB removal (reaction conditions: $Cd^{2+}$ and MB concentrations of 50 mg/L at 25 °C and pH 7, contact time are 40 min for $Cd^{2+}$ and 300 min for MB).**

At this stage, excessive adsorbents would cause agglomeration effects and insufficient metal ions could not fully occupy the adsorption sites, finally failing to reach the adsorption equilibrium. Therefore, 0.2 g/L was selected as the adsorbent dosage for the $Cd^{2+}$ and MB removal in the subsequent experiments.

2-3. Adsorption Kinetics

Adsorption is a time-dependent process and a reasonable adsorption time is essential for optimizing the overall experiment. The kinetics of adsorption help to determine the rate at which the solid phase adsorbs contaminant ions from the aqueous phase and brings the adsorption to equilibrium [11]. As shown in Fig. 7((a) and (b)), within the first 20 and 120 min, the adsorption capacities of XMBY for $Cd^{2+}$ and MB were very high but then slowly increased. After 40 and 300 min, the two adsorption processes reached equilibrium. During the initial stage, a large number of vacant binding sites were supplied for $Cd^{2+}$ and MB and rapid external surface adsorption occurred, which may be the decisive stage that determines the entire adsorption process [6]. During the late stage, the available binding sites were insufficient and a repulsive force emerged between the contaminant ions of the surface of the XMBY and the bulk solution, leading to a slow increase in the adsorption capacities [13]. Therefore, 40 and 300 min were selected for $Cd^{2+}$ and MB to study the adsorption equilibria in the following experiments. Furthermore, the pseudo-first-order model and pseudo-second-order model were applied to analyze the adsorption kinetic data. The two models are expressed as follows:

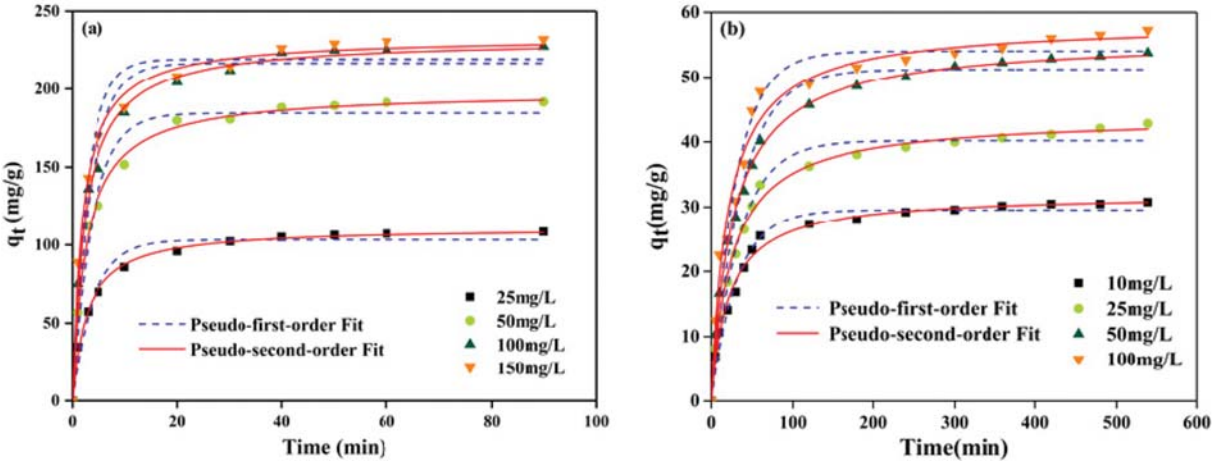


**Fig. 7. Adsorption kinetic curves for the adsorption of $Cd^{2+}$ (a) and MB (b) onto XMBY at different initial concentrations (reaction conditions: pH 7 for $Cd^{2+}$ and MB; XMBY dosage of 0.2 g/L; contact time are 90 min for $Cd^{2+}$ and 540 min for MB; 25 °C reaction temperature).**

**Table 1. Kinetic parameters for the adsorption of $Cd^{2+}$ and MB onto XMBY**

| Contaminant ions | $C_0$ (mg/L) | Experimental (mg/g) | Pseudo-first-order | | | Pseudo-second-order | | |
|---|---|---|---|---|---|---|---|---|
| | | | $q_e$ (mg/g) | $k_1$ ($min^{-1}$) | $R^2$ | $q_e$ (mg/g) | $k_2$ (g/mg·min) | $R^2$ |
| $Cd^{2+}$ | 25 | 108.5 | 103.25 | 0.2490 | 0.970 | 111.22 | 0.0033 | 0.997 |
| | 50 | 191.75 | 184.58 | 0.2611 | 0.974 | 198.38 | 0.0019 | 0.997 |
| | 100 | 227.5 | 216.8 | 0.2847 | 0.967 | 232.2 | 0.0018 | 0.996 |
| | 150 | 231.75 | 219.3 | 0.3496 | 0.961 | 233.3 | 0.0023 | 0.995 |
| MB | 10 | 30.75 | 29.54 | 0.0321 | 0.982 | 31.96 | 0.0015 | 0.991 |
| | 25 | 42.88 | 40.2 | 0.0290 | 0.984 | 43.87 | 0.0009 | 0.995 |
| | 50 | 53.25 | 51.21 | 0.0275 | 0.980 | 55.97 | 0.0006 | 0.998 |
| | 100 | 57 | 54.02 | 0.0332 | 0.968 | 58.33 | 0.0008 | 0.981 |

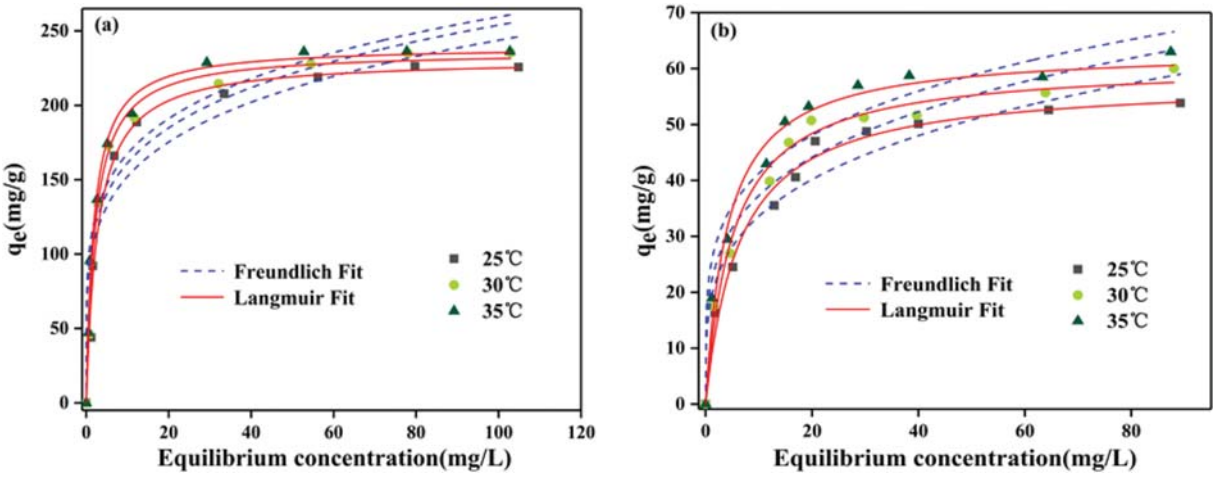


**Fig. 8. Adsorption isotherm curves for the adsorption of $Cd^{2+}$ (a) and MB (b) onto XMBY at different temperatures (reaction conditions: initial concentrations are 10 mg/L to 150 mg/L for $Cd^{2+}$ and 5 mg/L to 100 mg/L for MB with XMBY dosage of 0.2 g/L at pH 7; 25 °C, 30 °C, 35 °C reaction temperatures; contact time are 40 min for $Cd^{2+}$ and 300 min for MB).**

**Table 2. Isotherm parameters for the adsorption of $Cd^{2+}$ and MB onto XMBY**

| Contaminant ions | Temperature (°C) | Experimental (mg/g) | Langmuir model | | | Freundlich model | | |
|---|---|---|---|---|---|---|---|---|
| | | | $q_m$ (mg/g) | $K_L$ (L/mg) | $R^2$ | $K_F$ (mg/g) | n | $R^2$ |
| $Cd^{2+}$ | 25 | 225.75 | 231.36 | 0.360 | 0.980 | 95.01 | 4.887 | 0.893 |
| | 30 | 235.5 | 236.43 | 0.463 | 0.990 | 102.4 | 5.07 | 0.913 |
| | 35 | 236.25 | 239.8 | 0.541 | 0.990 | 108.14 | 5.261 | 0.912 |
| MB | 25 | 53.84 | 57.86 | 0.157 | 0.985 | 18.61 | 3.892 | 0.946 |
| | 30 | 60.02 | 60.91 | 0.193 | 0.986 | 21.29 | 4.106 | 0.949 |
| | 35 | 63 | 64.45 | 0.230 | 0.985 | 24.38 | 4.379 | 0.945 |

$$q_t = q_e(1-e^{-k_1 t}) \quad (3)$$

$$\frac{t}{q_t} = \frac{1}{k_2 q_e^2} + \frac{1}{q_e}t \quad (4)$$

where $q_t$ (mg/g) and $q_e$ (mg/g) are the adsorbed amount of $Cd^{2+}$ and MB at time t and at equilibrium, respectively; $k_1$ ($min^{-1}$) and $k_2$ (g/mg min) or $k_2$ (g $mg^{-1}$ $min^{-1}$) are the adsorption rate constants.

The final results of the kinetic data fitted by the pseudo-first-order model and the pseudo-second-order model are shown in Table 1. For different ion concentrations, the correlation coefficient values ($R^2$) obtained from the pseudo-second-order model exceeded those of the pseudo-first-order model. Moreover, the predicted values $q_e$ obtained from the pseudo-second-order model were also closer to the experimental values than the pseudo-first-order model. These results all indicate that the pseudo-second-order model better described the adsorption process and that the rate of the entire adsorption process was limited by chemisorption. In addition, the adsorption rate constants $k_2$ in the pseudo-second-order model were very low, indicating that the binding sites on the XMBY had a high affinity for both $Cd^{2+}$ and MB.

2-4. Adsorption Isotherms

The adsorption isotherms refer to the distribution of the adsorbate molecules between the solid phase and the liquid phase when the adsorption reaches equilibrium at a constant temperature [27]. Two typical isotherm equations were applied to fit the adsorption isotherm data; those are the Langmuir equation (Eq. (5)) and the Freundlich equation (Eq. (6)). The final fitted graphs and related data are shown in Fig. 8 and Table 2. The two isotherm equations are expressed as follows:

$$q_e = \frac{q_m K_L C_e}{1+K_L C_e} \quad (5)$$

$$q_e = K_F C_e^{1/n} \quad (6)$$

where $q_m$ (mg/g) is the maximum adsorption capacity, $C_e$ (mg/L) is the contaminant ion concentration at equilibrium, $K_L$ is the Langmuir constant, $K_F$ and n are the Freundlich constants related to the adsorption capacity and adsorption intensity, respectively.

Fig. 8((a) and (b)) shows that as the initial concentrations of $Cd^{2+}$ and MB increased, the adsorption capacities gradually increased as well, indicating that the higher the contaminant ion concentrations, the greater was the driving force; this makes it easier to overcome the mass transfer resistance present in the solution. Furthermore, at different temperatures for the same concentration, better adsorption performance was obtained at higher temperatures, which may have occurred because the higher temperature caused an increase in the diffusion rate of $Cd^{2+}$ and MB from the solution to the surface of the XMBY, thus promoting the adsorption capacities. The data in Table 2 show that the maximum values fitted by the Langmuir model are closer to the actual experimen-

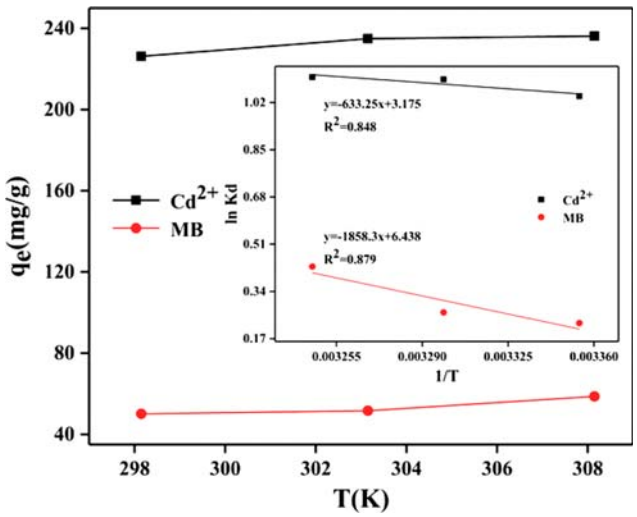


**Fig. 9. Effect of temperature on the adsorption capacities. Corresponding thermodynamic plot for the adsorption of $Cd^{2+}$ and MB onto XMBY is shown as an insert (reaction conditions: concentrations are 125 mg/L for $Cd^{2+}$ and 50 mg/L for MB, respectively; XMBY dosage of 0.2 g/L and pH 7; contact time are 40 min for $Cd^{2+}$ and 300 min for MB).**

tal values and the $R^2$ values are better than the fitted values of the Freundlich model. This demonstrates that the Langmuir model better describes the adsorption processes and also indicates that the adsorptions of $Cd^{2+}$ and MB onto the XMBY are mainly monolayer adsorption processes. The adsorption constant $K_L$ obtained from the Langmuir model gradually increased with increasing temperature. This further implied that the adsorption process was a chemical endothermic reaction and the adsorption intensity coefficient n exceeded 1, indicating a strong affinity between $Cd^{2+}$ or MB and the XMBY.

2-5. Thermodynamics Analysis

The effect of the temperature on the adsorption process cannot be ignored; therefore, the adsorption thermodynamics were studied and the obtained results are shown in Fig. 9 and Table 3. With increasing temperature ranging from 298.15 K to 308.15 K, the adsorption capacities for $Cd^{2+}$ and MB gradually increased from 226.25 to 236.25 mg/g and from 50.12 to 58.75 mg/g, respectively. This was because the higher temperature increased the collision efficiency between the adsorbate and the adsorbent; simultaneously, the deprotonation of the adsorption functional groups was enhanced, thus supplying more adsorption sites to the adsorbate. Moreover, the standard Gibbs free energy change (ΔG), standard entropy change (ΔS) and standard enthalpy change (ΔH) were reported to determine the adsorption nature. The specific expressions are displayed in Eq. (7) to Eq. (9) and the parameters are listed in Table 3:

$$k_d = \frac{q_e}{C_e} \tag{7}$$

$$\Delta G = -RT\ln K_d \tag{8}$$

$$\ln K_d = -\frac{\Delta H}{RT} + \frac{\Delta S}{R} \tag{9}$$

where $k_d$ (L/g) is the adsorption equilibrium constant, $q_e$ (mg/g) is the adsorption capacity at a certain temperature, $C_e$ (mg/L) is the ion concentration remaining in the solution. R is the gas constant (8.314 J/mol·K), T is the Kelvin temperature (K). The values of ΔH and ΔS can be calculated from the slope and intercept, respectively.

The values of ΔG were all -20-0 KJ/mol for all temperatures, demonstrating that the adsorption process was spontaneous [31]. When the temperature increased from 298.15 to 318.15 K, $k_d$ and the absolute values of ΔG gradually increased, indicating that the spontaneity degrees of the chemisorption processes of $Cd^{2+}$ and MB onto XMBY were enhanced. The values of ΔH were above zero, which indicated that the adsorption processes were endothermic. The positive values of ΔS showed that the randomness of the solid-solution interface increased during the adsorption process, which may be because the coordination water molecules were displaced by $Cd^{2+}$ and MB, resulting in an increase in the randomness of the adsorbent-contaminant system [28].

### 3. Interactions in the Binary-component ($Cd^{2+}$ and MB) Solution

As mentioned, wastewaters typically contain more than one type of pollutant. Therefore, an adsorbent with excellent performance is not only suitable for a single-component pollutant but may also work effectively in a binary-component or a multi-component pollutant system [30]. In wastewater that contains heavy metal ions and dye ions, the physical and chemical properties may differ considerably from those of a single-component pollutant system. Hence, it is of great practical significance to study the adsorption mechanism of adsorbents in a binary-component system. In this section, we focused on the XMBY to investigate the adsorption performance in a $Cd^{2+}$-MB (or MB-$Cd^{2+}$) system and to explore the underlying adsorption mechanism. The effects of the initial contaminant concentrations on the adsorption of $Cd^{2+}$ and MB onto XMBY were investigated in a binary-component system and the results

**Table 3. Thermodynamic parameters for the adsorption of $Cd^{2+}$ and MB onto XMBY**

| Contaminant ions | Temperature (°C) | $K_d$ ($cm^3$/g) | ΔG (kJ/mol) | ΔH (kJ/mol) | ΔS (J $mol^{-1}$ $K^{-1}$) |
|---|---|---|---|---|---|
| $Cd^{2+}$ | 25 | 2.837 | −2.585 | 5.265 | 26.397 |
| | 30 | 3.013 | −2.780 | | |
| | 35 | 3.039 | −2.847 | | |
| MB | 25 | 1.254 | −0.561 | 15.449 | 53.526 |
| | 30 | 1.303 | −0.666 | | |
| | 35 | 1.536 | −1.099 | | |

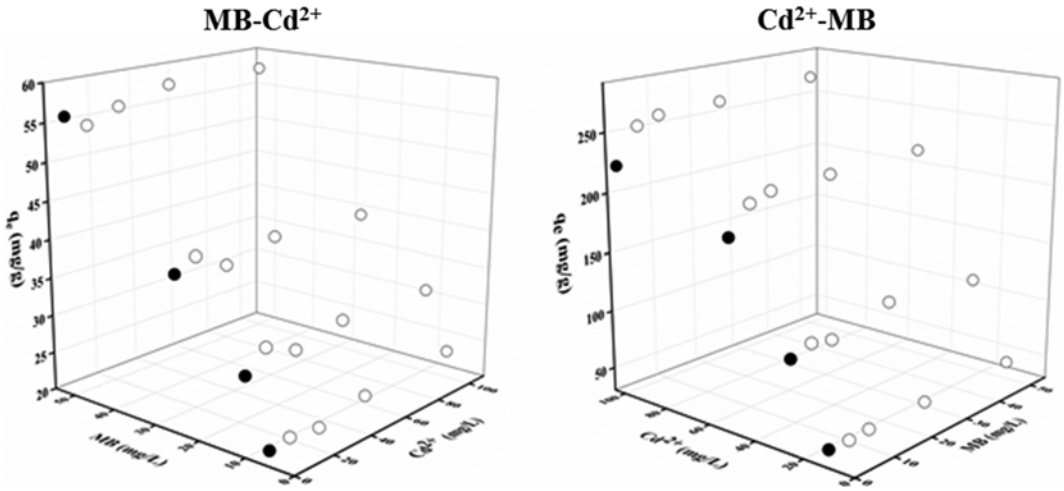


**Fig. 10. Effect of initial contaminant ion concentration on the adsorption of $Cd^{2+}$ and MB onto XMBY in binary-component system. (●) Single-component and (○) binary-component system (reaction conditions: initial concentrations of 10, 25, 50 and 100 mg/L for $Cd^{2+}$ and 5, 10, 25 and 50 mg/L for MB; XMBY dosage of 0.2 g/L and pH 7; contact time are 40 min for $Cd^{2+}$-MB system and 300 min for MB-$Cd^{2+}$ system; 25 °C reaction temperature).**

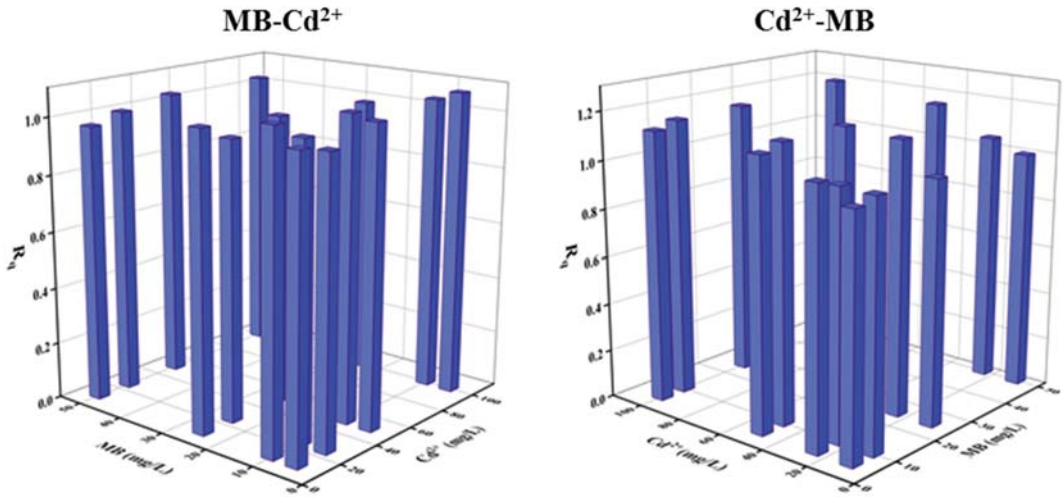


**Fig. 11. Ratio of adsorption capacity ($R_q$) versus the initial concentration in binary-component system for the simultaneous removal of $Cd^{2+}$ and MB using XMBY.**

are shown in Fig. 10. The effects of both $Cd^{2+}$ and MB in a binary-component system on the removal performance of XMBY were also studied via the ratio of the adsorption capacities ($R_q$). The obtained results are shown in Fig. 11.

$$R_q = \frac{q_{e,i}}{q_{0,i}} \tag{10}$$

where $q_{e,i}$ and $q_{0,i}$ are the adsorption capacities for contaminant i in the binary-component system and single-component system. Previous literature has reported that if $R_q$>1, the adsorption of contaminant i was promoted by the other contaminants; if $R_q$=1, there is no effect on the adsorption capacity of contaminant i; if $R_q$<1, the adsorption of contaminant i was suppressed by the other contaminant [5].

3-1. Interactions in the MB-$Cd^{2+}$ System

As seen in Fig. 10, at initial concentrations of 50 mg/L for $Cd^{2+}$ and 10 mg/L for MB, the adsorption capacities for MB in single-component and binary-component systems were 30.13 mg/g and 32 mg/g, respectively. The concentration of $Cd^{2+}$ remained unchanged at 50 mg/L, but the concentration of MB increased from 10 mg/L to 50 mg/L. The adsorption capacities for MB were 56.25 mg/g in the single-component system and 57.88 mg/g in the binary-component system. This indicated that with increasing concentrations of MB, the adsorption capacity for MB onto XMBY was not strongly affected by the presence of $Cd^{2+}$ and the variation of the adsorption capacity was small. The concentration of MB remained unchanged at 10 mg/L and the concentrations of $Cd^{2+}$ increased from 50 mg/L to 100 mg/L. The adsorption capacities for MB were 32 mg/g and 31.38 mg/g in the single-component and binary-component systems, respectively and the $R_{q,MB}$ value of the latter (1.041) did not change much compared to the former (1.062). All values of $R_{q,MB}$ were in the range of 0.975 to 1.075 and most values were

close to 1. This showed that in the binary-component system, regardless of whether the amount of $Cd^{2+}$ ions increased, the influence of the presence of $Cd^{2+}$ ions on MB adsorption was limited.

This may be because, during the adsorption process, metal ions interacted with the single pair of electrons in the amino groups and chelated with most of the sulfur groups. In addition, electrostatic adsorption with hydroxyl groups and ion exchange processes also occurred. Furthermore, a small portion of the sulfur groups and hydroxyl groups electrostatically reacted with the dye ions. During the entire adsorption process, the groups that primarily reacted with the metal ions and dye ions were different and the metal ion adsorption process was relatively independent. When the adsorption process was completed, the metal ions tended to be stable in the binary-component system; therefore, this did not exert a large influence on the adsorption process of the dyes.

3-2. Interactions in the $Cd^{2+}$-MB System

Interestingly, the adsorption behavior for $Cd^{2+}$ differed in binary-component system. For most matching concentrations, the adsorption of $Cd^{2+}$ onto XMBY increased in the presence of MB, and the adsorption capacity further increased with increasing MB concentrations (Fig. 10). At an initial $Cd^{2+}$ concentration of 50 mg/L and 50 mg/L for MB, the adsorption capacity for $Cd^{2+}$ was 188 mg/g in the single-component system and 216.25 mg/g in the binary-component system, respectively. When the $Cd^{2+}$ concentration was 100 mg/L, the concentration of MB remained unchanged at 50 mg/L and the adsorption capacity for $Cd^{2+}$ increased from 224.5 mg/g in the single-component system to 267 mg/g in the binary-component system. This indicates that when the concentration of MB was constant, the change trend of the adsorption capacity was identical to that in the single-component system: the adsorption capacity increased with increasing initial concentrations of $Cd^{2+}$. Furthermore, the increment ratio increased from 15.03% to 18.93%, which clarified that the presence of MB promoted the adsorption of $Cd^{2+}$ onto the surface of the XMBY. When the concentration of $Cd^{2+}$ was maintained at 50 mg/L, the concentration of MB increased from 5 mg/L to 50 mg/L, the adsorption capacity for $Cd^{2+}$ increased from 209.75 mg/g to 216.25 mg/g, and the increment ratio increased from 11.57% to 15.03%. This indicates that the presence of MB not only exerted a synergistic effect on the adsorption of $Cd^{2+}$ but the higher concentrations of MB had a more significant effect on the adsorption of $Cd^{2+}$ onto XMBY. This occurred because the metal ions chelated with the dyes in response to the electrostatic interactions between the XMBY and dyes. In other words, additional binding sites were supplied to the metal ions during this process. The higher the number of dye ions, the more apparent the effect was; therefore, the adsorption capacity for $Cd^{2+}$ onto XMBY increased.

Furthermore, we also observed that when the concentration of $Cd^{2+}$ was maintained at 50 mg/L, the concentration of MB increased from 5 mg/L to 50 mg/L and the adsorption capacity for $Cd^{2+}$ did not increase significantly (209.75 mg/g to 216.25 mg/g with an increment ratio of 3.1%). Therefore, we repeated the experiment in triplicate to eliminate any errors again; the results showed that the low increments of the adsorption capacities were normal. In addition, we conducted another set of experiments. When the concentration of MB was maintained at 5 mg/L, the concentration of $Cd^{2+}$ increased from 50 mg/L to 100 mg/L and the adsorption capacity increased from 209.75 mg/g to 233.5 mg/g (increment ratio of 11.32%) in the binary-component system. Compared with the previous set of experiments (50 mg/L for $Cd^{2+}$ and 50 mg/L for MB), the increment ratio of the adsorption capacity in the binary-component system was larger than the previous comparison (11.32% and 3.1%). These results indicate that when the $Cd^{2+}$ concentration is relatively low, the MB ions in the aqueous solution will occupy some of the specific binding sites for $Cd^{2+}$. However, during the adsorption process, the additional binding sites provided by the MB to $Cd^{2+}$ are limited, which results in an unobvious increment in the adsorption capacity for $Cd^{2+}$.

To intuitively represent the adsorption behavior in the binary-component system, the changes in $R_{q,Cd}^{2+}$ at different initial concentrations of $Cd^{2+}$ and MB are compared in Fig. 11. The values of $R_{q,Cd}^{2+}$ ranged from 0.988 to 1.189 and most values exceeded 1, which further illustrated that the presence of MB had a positive impact on the adsorption capacity for $Cd^{2+}$ in the binary-component system. In previous literature, similar phenomena have also been reported; EDTA-cross-linked $\beta$-cyclodextrin was utilized by Zhao

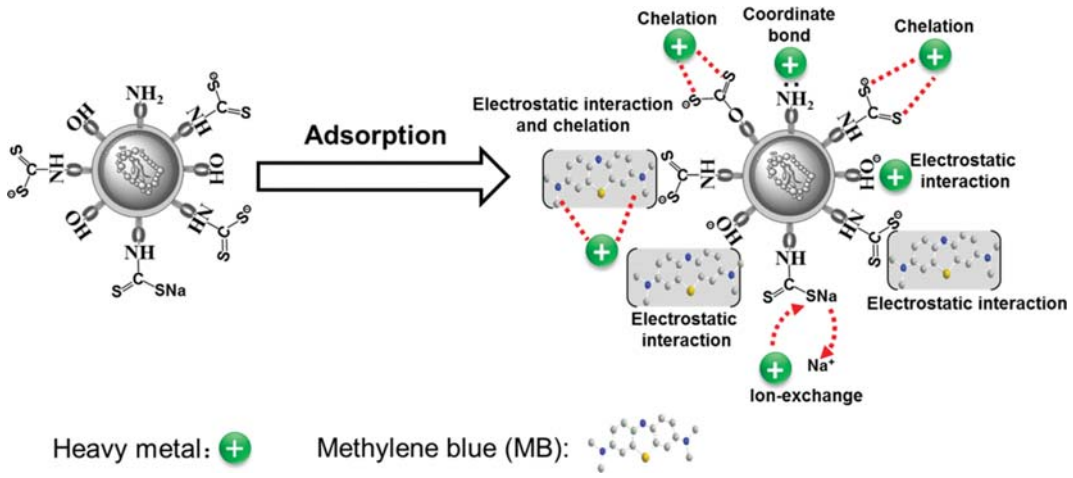


**Fig. 12. Proposed mechanism for the simultaneous removal of heavy metals and dyes by XMBY.**

et al. for adsorbing $Cu^{2+}$, $Cd^{2+}$, MB, SO, and CV [3] and $Ca(PO_3)_2$-modified carbon was used by Tovar et al. for adsorbing $Zn^{2+}$, $Ni^{2+}$, $Cd^{2+}$, and AB25 [33]. The obtained results showed that the adsorption capacities for the metals were significantly improved by the presence of dyes.

A proposed mechanism for the simultaneous removal of $Cd^{2+}$ and MB by the XMBY is depicted in Fig. 12.

## CONCLUSION

Biosorbent XMBY was successfully synthesized. The characterization of the XMBY by SEM-EDS and FTIR revealed the introduction of sulfur groups during the modification process. The kinetic data were best fitted by the pseudo-second-order model. The obtained equilibrium time and adsorption capacity were 40 min and 233.30 mg/g, respectively, at an initial concentration of 150 mg/L for $Cd^{2+}$ and 300 min and 58.33 mg/g, respectively, at an initial concentration of 100 mg/L for MB. The isotherm data fitted the Langmuir model well and the maximum values were 239.80 mg/g for $Cd^{2+}$ and 64.45 mg/g for MB at 35 °C. With regard to the thermodynamic data, the standard free energy (ΔG) and standard entropy (ΔH) indicated that the adsorption process was spontaneous and endothermic. In the binary-component system, the adsorption capacity for MB was almost unaffected by the presence of $Cd^{2+}$; however, the adsorption capacity for $Cd^{2+}$ increased in the presence of MB because the metal chelated with the dye in response to the electrostatic interactions between the XMBY and the dye. The low raw material price, simple preparation, and great adsorption performance indicate that XMBY is an excellent adsorbent for the treatment of wastewater that contains both $Cd^{2+}$ and MB.

## ACKNOWLEDGEMENTS

We would like to acknowledge the National Natural Science Foundation of China (Project No. 41867031) for the fund support to carry out this work.

## REFERENCES

1. B. K. Körbahti, K. Artut, C. Geçgel and A. Ozer, *Chem. Eng. J.*, **173**, 677 (2011).
2. M. Visa, C. Bogatu and A. Duta, *Appl. Surf. Sci.*, **256**, 5486 (2010).
3. F. P. Zhao, E. Repo, D. L. Yin, Y. Meng, S. Jafari and M. Sillanpaa, *Environ. Sci. Technol.*, **49**, 10570 (2015).
4. G. Z. Kyzas, P. I. Siafaka, E. G. Pavlidou, K. J. Chrissafis and D. N. Bikiaris, *Chem. Eng. J.*, **259**, 438 (2015).
5. J. H. Deng, X. R. Zhang, G. M. Zeng, J. L. Gong, Q. Y. Niu and J. Liang, *Chem. Eng. J.*, **226**, 189 (2013).
6. L. M. Cui, X. Y. Guo, Q. Wei, Y. G. Wang, L. Gao, L. G. Yan, T. Yan and B. Du, *J. Colloid Interface Sci.*, **439**, 112 (2015).
7. F. L. Fu and Q. Wang, J. *Environ. Manage.*, **92**, 407 (2011).
8. S. Chaouchi and O. Hamdaoui, *Sep. Purif. Technol.*, **129**, 32 (2014).
9. Q. Li, H. J. Su, J. Li and T. W. Tan, *Process Biochem.*, **42**, 379 (2007).
10. G. C. Panda, S. K. Das and A. K. Guha, *Colloid Surf. B-Biointerfaces.*, **62**, 173 (2008).
11. S. Liang, X. Y. Guo, N. C. Feng and Q. H. Tian, *J. Hazard. Mater.*, **170**, 425 (2009).
12. E. A. Deliyanni, E. N. Peleka and K. A. Matis, *J. Hazard. Mater.*, **141**, 176 (2007).
13. S. S. Pillai, B. Deepa, E. Abraham, N. Girija, P. Geetha, L. Jacob and M. Koshy, *Ecotox. Environ. Safe.*, **98**, 352 (2013).
14. J. Y. Liu, C. W. Hu and Q. G. Huang, *Bioresour. Technol.*, **271**, 487 (2019).
15. G. C. Zhu, J. F. Liu, J. Yin, Z. W. Li, B. Z. Ren, Y. J. Sun, P. Wan and Y. S. Liu, *Chem. Eng. J.*, **288**, 390 (2016).
16. M. A. Al-Ghouti, J. Li, Y. Salamh, N. Al-Laqtah, G. Walker and M. N. M. Ahmad, *J. Hazard. Mater.*, **176**, 510 (2010).
17. V. Padmavathy, *Bioresour. Technol.*, **99**, 3100 (2008).
18. J. X. Yu, B. H. Li, X. M. Sun, Y. Jun and R. A. Chi, *Biochem. Eng. J.*, **45**, 145 (2009).
19. Y. X. Xia, L. Y. Meng, Y. J. Jiang, Y. S. Zhang, X. X. Dai and M. J. Zhao, *Chem. Eng. J.*, **259**, 927 (2015).
20. C. Li, X. J. Wang, D. Y. Meng and L. Zhou, *Int. J. Biol. Macromol.*, **107**, 1871 (2018).
21. Y. H. Song, J. S. Tan, G. Wang and L. Zhou, *Carbohydr. Polym.*, **199**, 178 (2018).
22. J. K. Bediako, W. Wei, S. Kim and Y.-S. Yun, *J. Hazard. Mater.*, **299**, 550 (2015).
23. L. Sun, H. W. Yu and B. S. Fugetsu, *J. Hazard. Mater.*, **203**, 101 (2012).
24. M. Srinivasan, C. Ferraris and T. White, *Environ. Sci. Technol.*, **40**, 7054 (2006).
25. L. Zhou, J. Jin, Z. Liu, X. Liang and C. Shang, *J. Hazard. Mater.*, **185**, 1045 (2011).
26. B. Kannamba, K. L. Reddy and B. V. Apparao, *J. Hazard. Mater.*, **175**, 939 (2010).
27. G. X. Zhao, J. X. Li and X. K. Wang, *Chem. Eng. J.*, **173**, 185 (2011).
28. A. Baraka, P. J. Hall and M. J. Heslop, *React. Funct. Polym.*, **67**, 585 (2007).
29. W. S. Wan Ngah, L. C. Teong and M. A. K. M. Hanafiah, *Carbohydr. Polym.*, **83**, 1446 (2011).
30. M. Lu, Y. G. Liu, X. J. Hu, Y. Ben, X. X. Zeng, T. T. Li and H. Wang, *J. Cent. South Univ.*, **20**, 2478 (2013).
31. J. Ma, F. Yu, L. Zhou, L. Jin, M. X. Yang, J. S. Luan, Y. H. Tang, H. B. Fan, Z. W. Yuan, J. H. Chen, *ACS Appl. Mater. Interfaces.*, **4**, 5749 (2012).
32. Y. Li, A. H. Lu, S. Jin and C. Q. Wu, *J. Hazard. Mater.*, **170**, 479 (2009).
33. R. Tovar-Gomez, D. A. Rivera-Ramirez, V. Hernandez-Montoya, A. Bonilla-Petriciolet, C. J. Duran-Valle and M. A. Montes-Moran, *J. Hazard. Mater.*, **199**, 290 (2012).
34. B. Huang, M. C. Lu, D. L. Wang, Y. H. Song and L. Zhou, *Carbohydr. Polym.*, **181**, 785 (2018).